Phytochemistry 216 (2023) 113890

Contents lists available at ScienceDirect

Phytochemistry

journal homepage: www.elsevier.com/locate/phytochem

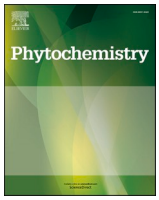

Phukettosides A–E, mono- and bis-iridoid glycosides, from the leaves of *Morinda umbellata* L

Wirongrong Kaweetripob [a], Sanit Thongnest [a,d], Jutatip Boonsombat [a,d], Paratchata Batsomboon [b], Abdul-Wahab Salae [e], Hunsa Prawat [a,d,*], Chulabhorn Mahidol [a,c], Somsak Ruchirawat [b,c,d]

[a] Laboratory of Natural Products, Chulabhorn Research Institute, Bangkok, 10210, Thailand
[b] Laboratory of Medicinal Chemistry, Chulabhorn Research Institute, Bangkok, 10210, Thailand
[c] Program in Chemical Sciences, Chulabhorn Graduate Institute, Chulabhorn Royal Academy, Bangkok, 10210, Thailand
[d] Center of Excellence on Environmental Health and Toxicology (EHT), OPS, MHESI, Thailand
[e] Laboratory of Natural Products Chemistry, Faculty of Science and Technology, Phuket Rajabhat University, Muang, Phuket 83000, Thailand

ARTICLE INFO

Keywords:
Morinda umbellata
Rubiaceae
Iridoid glycoside
Bis-iridoid glycoside
Flavonoid
Diels-Alder cycloaddition
Antioxidant
Cytotoxic activity

ABSTRACT

Four undescribed bis-iridoid glycosides, named phukettosides A–D, and one iridoid glycoside, referred to as phukettoside E, were isolated and fully characterized from the leaves of *Morinda umbellata* L. Phytochemical analysis also revealed the presence of eight known compounds. The structures were determined through extensive analysis of 1D and 2D-NMR spectroscopic and HRMS spectral data, and the absolute configurations of the isolates were deduced through ECD calculations. Biogenetic pathways for the bis-iridoid glycosides, phukettosides A–C, through intermolecular Diels-Alder type reactions, were proposed. The isolated compounds, with the exception of phukettosides B and D, were evaluated against a panel of cancer cell lines (MOLT-3, HuCCA-1, A549, HeLa, HepG2, and MDA-MB-231) and a non-cancerous cell line (MRC-5) for their cytotoxicity. None of the isolates had significant cytotoxic effects on the tested cell lines.

1. Introduction

The genus *Morinda* L. belongs to the family Rubiaceae and comprises about 40 species, distributed mainly in the pantropical regions (Razafimandimbison and Bremer, 2011), and parts of these plants have been widely used in traditional medicine against several diseases (Oladeji et al., 2022). Phytochemically, *Morinda* plants are rich sources of anthraquinones (Chang and Chen, 1995; Li et al., 2019, 2021, 2022), flavonoid glycosides (Akihisa et al., 2007; Hashim et al., 2021; Sang et al., 2001; Su et al., 2005), lignans (Deng et al., 2007; Hashim et al., 2021), saccharide fatty acid esters (Akihisa et al., 2007; Dalsgaard et al., 2006), iridoids (Akihisa et al., 2007; Ban et al., 2013; Cai et al., 2021; Hashim et al., 2021; Kanchanapoom et al., 2002; Sang et al., 2001), secoiridoids (Cai et al., 2021; Zandi et al., 2020), and iridoid dimers (Sang et al., 2003). They possess various pharmacological effects, including lipoxygenase inhibition (Deng et al., 2007), cytotoxicity (Ban et al., 2013; Chiou et al., 2014; Li et al., 2019, 2021, 2022), anti-malarial activity (Hashim et al., 2021), antioxidant activity (Sang et al., 2001; Su et al., 2005), and anti-inflammatory properties (Akihisa et al., 2007; Cai et al., 2021).

Morinda umbellata L., commonly known as "Yo yaan" in Thai, is one of approximately 15 species and 3 varieties of *Morinda* plants found in Thailand (Kesonbuaa and Chantaranothai, 2013). The plant has been extensively used in many countries, including China, India, Vietnam, and Thailand, as a traditional medicine to treat diseases such as diarrhea, dysentery, furuncle, skin diseases, and rheumatism (Ban et al., 2013; Chiou et al., 2014; Ismail and Sulthana, 2008). The leaf powder exhibited antioxidant and antileukemic effects (Ismail and Sulthana, 2008), and the vine stem extract showed cytotoxic activity (Chang and Chen, 1995). Moreover, the aerial parts show modest cytotoxic activity against the human colorectal cancer cell line HCT116 (Li et al., 2019). Phytochemical studies of *M. umbellata* have revealed that anthraquinones are the major chemical constituents (Burnett and Thomson, 1968; Chang and Chen, 1995; Chiou et al., 2014; Li et al., 2019, 2021, 2022) in addition to phenols (Li et al., 2022), sesquiterpenes (Li et al., 2022), and iridoids (Ban et al., 2013).

* Corresponding author. Laboratory of Natural Products, Chulabhorn Research Institute, Bangkok, 10210, Thailand.
E-mail address: hunsa@cri.or.th (H. Prawat).

https://doi.org/10.1016/j.phytochem.2023.113890
Received 7 June 2023; Received in revised form 5 October 2023; Accepted 7 October 2023
Available online 16 October 2023
0031-9422/

Herein, four previously undescribed bis-iridoid glycosides and one monomer, together with eight known compounds are reported from the CH_2Cl_2−MeOH (1:1, v/v) extract of the leaves of *M. umbellata*. Biogenetic pathways for the bis-iridoid glycosides were proposed to occur through intermolecular Diels-Alder type reactions. Notably, this study describes the occurrence of this type of dimer in a natural iridoid glycoside for the first time. Bioassays probing the potential cancer chemopreventive activity and cytotoxicity of the isolates were performed.

2. Results and discussion

The crude 1:1 CH_2Cl_2−MeOH extract of *M. umbellata* leaves was divided into six fractions (A–F) by silica gel column chromatography. All fractions were screened for the presence of iridoids and flavonoids through ^{1}H-NMR experiments. Fraction C displayed signals characteristic of iridoids (δ_H 5.5–7.8 ppm) in the ^{1}H-NMR spectrum (Fig. S1), while fraction E exhibited signals characteristic of flavonoids (δ_H 6.0–8.0 ppm) (Fig. S2). Since iridoids and flavonoids have extensive biological activities (Dinda et al., 2011; Sang et al., 2001), and the leaf powder of *M. umbellata* possesses antioxidant effects (Ismail and Sulthana, 2008), fractions C and E were further purified by repeated chromatography, yielding seven iridoid glycosides and three flavonoid glycosides (Fig. 1).

Compound **1** was obtained as a pale-yellow gum ($[\alpha]_D^{26}$ −75.0, *c* 0.46, MeOH). The molecular formula was established as $C_{33}H_{46}O_{18}$ from the HRESIMS *m/z* 753.2585 $[M + Na]^+$ (calcd for $C_{33}H_{46}NaO_{18}$ 753.2576) and the NMR data, which suggested eleven degrees of unsaturation. The IR spectrum indicated the presence of hydroxy (3359 cm^{-1}), ester carbonyl (1704 cm^{-1}), and γ-lactone carbonyl (1741 cm^{-1}) groups. The ^{13}C-NMR and DEPT spectra, combined with the HSQC spectra (Table 1), revealed 33 carbons in the form of two carbonyl (one acetoxy and one lactone), four olefinic, 18 oxygenated (two sets of glucose, three methylene, two methine, one acetal), three methine, two methylene, two methyl (one alkyl, one acetoxy), and two quaternary carbons. Extensive analysis of the NMR data indicated that **1** consisted of two molecular units: asperuloside (**7**) (Demirezer et al., 2006; Noiarsa et al., 2008; Otsuka et al., 1991), an iridoid glycoside in unit **A**, and kankanoside D (**14**) (Xie et al., 2006), an 11-nor-iridoid glycoside in unit **B**. The HMBC correlations from H-1 (δ_H 4.46, d, J = 9.0 Hz) to C-3 (δ_C 87.0), C-8 (δ_C 149.5), and C-1′ (δ_C 100.1), from H-3 (δ_H 4.55, d, J = 4.0 Hz) and H-5 (δ_H 3.19, dd, J = 9.7, 7.8 Hz) to C-11 (δ_C 181.7), from H-9 (δ_H 2.77, t, J = 9.2 Hz) to C-4 (δ_C 55.3), C-6 (δ_C 86.9), and C-7 (δ_C 125.9), and from H-1' (δ_H 4.61, d, J = 7.9 Hz) to C-1 (δ_C 101.1) were observed, thus establishing the presence of a 3,4-saturated iridoid glycoside in unit **A**. The remaining 15 carbon signals were attributed to the kankanoside D unit (unit **B**). However, significant spectroscopic differences associated with the original cyclopentene ring of kanakanoside D were observed. The key HMBC correlations from H_2-3" (δ_H 4.02, dt, J = 9.8, 6.5 Hz and δ_H 3.71, dt, J = 9.8, 6.9 Hz) and H_2-7" (δ_H 2.20, d, J = 8.6 Hz and δ_H 1.43, dd, J = 8.6, 1.5 Hz) to C-5" (δ_C 149.0), and from H_3-10" (δ_H 1.29) and H_2-7" to C-9" (δ_C 145.0) suggested a double bond between C-5" and C-9", and hence the unit was proposed to be derived from the allylic hydroxylation and dehydration product of kankanoside D (Scheme 1). Detailed 1D and 2D-NMR spectroscopic data (DEPT, COSY, HSQC, HMBC, ROESY and NOESY) indicated the connectivity of five fragments (**a**–**e**) (Fig. 2) and seven quaternary carbons, thus establishing the molecular structure of **1**. Specifically, the HMBC correlations from H-3 (δ_H 4.55, d, J = 4.0 Hz) to C-5" (δ_C 149.0), C-6" (δ_C 50.2), C-7" (δ_C 49.6), and C-8" (δ_C 62.4), from H_2-7" to C-3 (δ_C 87.0) and C-4 (δ_C 55.3), and from H_3-10" to C-4 (Fig. 2) indicated the connections of the asperuloside unit **A** and the kankanoside D unit **B** to be through two C–C bonds, one between C-3 and C-6" and another between C-4 and C-8" (red bonds, Fig. 1). The relative configuration of **1** was established by analysis of key correlations observed in the ROESY (CD_3OD) and NOESY (DMSO-d_6) spectra (Fig. 2). Additionally, the coupling constants of *cis* H5/H9β and *cis* H-5/H-6 from the experimental ^{1}H-NMR data were compared with the calculated ^{1}H-NMR data (Table S13), and showed consistency. In the ROESY and NOESY spectra (Fig. 2), correlations of H-5/H-6, H-5/H-9, H-5/H_2-1", H-1/H-3, and H-3/H-7" indicated that H-5, H-6, H-9, and H-1" were on the β-face, which corresponded to the structural characteristics of naturally occurring iridoids with a β-*cis*-fused (H-5/H-9β) ring juncture (Dinda et al., 2011). Additionally, the orientation on the α-face was determined for H-1, H-3, and H-7". Acid hydrolysis of **1** gave D-glucose, which was identified by TLC comparison with an authentic sample and by comparison of optical rotation data. The large coupling constant values of the anomeric protons ($J_{1',2'}$ = 7.9, $J_{1''',2'''}$ = 7.8 Hz) suggested a β-glucosidic linkage within each unit. The absolute configuration of **1** was defined by comparing the experimental ECD spectra with the calculated spectra (Fig. 3a). Based on this analysis, the absolute configuration for compound **1** was established as 1*S*,3*R*,4*R*,5*S*,6*S*,9*S*,6"*S*, 8"*R*, and **1** was named phukettoside A.

Compound **2** was obtained as a pale-yellow gum with $[\alpha]_D^{26}$ −71.3 and was assigned the molecular formula $C_{33}H_{46}O_{18}$, based on the HRESIMS data (*m/z* 765.2367 $[M + Cl]^-$, calcd for $C_{33}H_{46}O_{18}Cl$ 765.2378), together with the NMR spectroscopic data, which indicated eleven indices of hydrogen deficiency. Detailed analysis of the NMR data for **1** and **2** (Table 1) showed that they shared the same planar structure, except for their relative configurations. The ROESY correlation of H-5/H-7" in compound **2** (Fig. 4) confirmed that it was an *exo* product resulting from the Diels-Alder cycloaddition of the diene (int-**1**), derived from the allylic hydroxylation and dehydration product of kankanoside D (**14**), with the dienophile asperuloside (**7**) (Scheme 1). The relative configuration of **2** was further determined by the ROESY spectrum (Fig. 4). The assigned *cis* H5/H9β and *cis* H-5/H-6 were confirmed by comparing the coupling constants of the experimental ^{1}H-NMR data with the calculated ^{1}H-NMR data (Table S14), which showed consistency. The cross peaks of H-5/H-6, H-5/H-9, H-5/H_2-7″, and H-1/H-3 indicated that H-5, H-6, H-9, and H-7″ were on the β-face, while H-1 and H-3 were on the α-face. This characterization indicated that the product retains the stereochemistry of asperuloside (**7**), and that **2** can be defined as an *exo* product. The absolute configuration of **2** was established as 1*S*,3*R*,4*R*,5*S*,6*S*,9*S*,6"*R*,8"*S* based on comparison of the experimental and calculated ECD spectra (Fig. 3b) and the isolate **2** was named phukettoside B.

Compound **3** was obtained as a pale-yellow gum showing $[\alpha]_D^{26}$ −56.8. Its molecular formula was established as $C_{33}H_{46}O_{18}$ from the HRESIMS *m/z* 753.2573 $[M + Na]^+$ (calcd for $C_{33}H_{46}NaO_{18}$ 753.2576). The NMR spectroscopic data of **3** were similar to those of **1** and **2**, except for different carbon linkages between the monomer units. The ^{13}C-NMR shifts (Table 1) of C-5"–C-9" were different from those of the corresponding carbons in **1**, which were shifted from δ_C 149.0 to 65.2 (C-5"), 50.2 to 45.1 (C-6"), 49.6 to 51.7 (C-7"), 62.4 to 150.0 (C-8"), and 145.0 to 140.8 (C-9"), respectively, indicating a different linkage for unit **B**. The ^{1}H-^{1}H COSY data established the linkage of H-3/H-7" (Fig. 5. Further proof of this structure resides in the HMBC ^3J cross peaks from H-3 (δ_H 4.53, d, J = 3.9 Hz) to C-8" (δ_C 150.0) and C-5" (δ_C 65.2), from H-5 (δ_H 3.22, dd, J = 9.7, 7.6 Hz) to C-5" (δ_C 65.2), from H_2-4" (δ_H 2.27, ddd, J = 13.6, 8.5, 5.3 Hz and 1.82, ddd, J = 13.6, 9.0, 7.0 Hz) to C-4 (δ_C 55.9), from H-7" (δ_H 2.96) to C-10" (δ_C 15.8), and from H_3-10" (δ_H 1.91) to C-7" (δ_C 51.7), confirming the connection of units **A** and **B** between C-3/C-7" and C-4/C-5" (Fig. 5). The relative configuration of **3** was determined by the NOESY (DMSO-d_6) and ROESY (CD_3OD) spectra. The strong NOE correlations of H-1/H-3 and H3/H-6″ revealed that they were on the same face and were assigned as α-oriented, whereas the correlations of H-5/H-6 and H-5/H-9 indicated that they were on the opposite side and were allocated as β-oriented. The assignment of *cis* H5/H9β and *cis* H-5/H-6 was confirmed by comparing the coupling constants obtained from experimental ^{1}H-NMR data with the calculated ^{1}H-NMR data (Table S15). The comparison revealed a consistent match

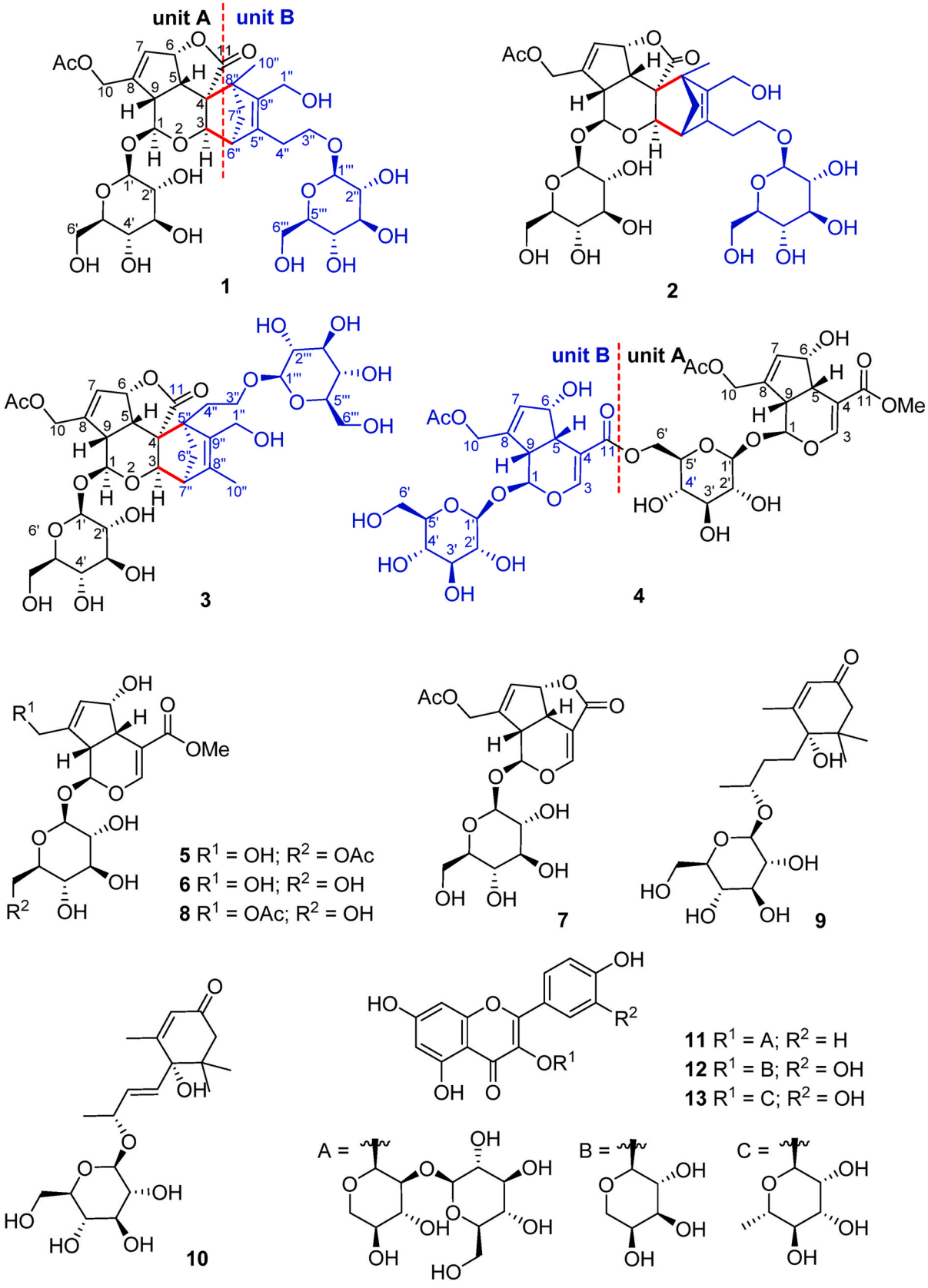

Fig. 1. Structures of compounds **1**–**13**.

Table 1
^{1}H- (600 MHz) and ^{13}C-NMR (150 MHz) NMR spectroscopic data[a] for compounds **1**–**3** in CD_3OD (δ in ppm, J in Hz).

Position	1		2		3	
	δ_C	δ_H, mult. (J)	δ_C	δ_H, mult. (J)	δ_C	δ_H, mult. (J)
unit A						
1	101.1	4.46, d (9.0)	100.8	4.47, d (9.0)	101.1	4.45, d (8.9)
3	87.0	4.55, d (4.0)	86.0	3.97, s	87.0	4.53, d (3.9)
4	55.3	–	54.8	–	55.9	–
5	44.4	3.19, dd (9.7, 7.8)	44.6	3.30, o	44.5	3.22, dd (9.7, 7.6)
6	86.9	5.33, br d (7.5)	86.8	5.35, d (7.2)	86.8	5.34, d (7.1)
7	125.9	5.94, m	125.9	5.96, s	125.9	5.94, br s
8	149.5	–	149.0	–	149.5	–
9	49.3	2.77, t (9.2)	49.6	3.05, t (9.3)	49.1	2.74, t (9.3)
10	63.3	4.93, d (16.2)	63.2	5.00, d (16.1)	63.3	4.92, d (15.6)
		4.67, d (16.2)		4.70, d (16.1)		4.68, d (15.6)
10-O$\underline{C}$OCH$_3$	172.5	–	172.6	–	172.5	–
10-OCO$\underline{CH_3}$	20.7	2.10, s	20.7	2.11, s	20.7	2.10, s
11	181.7	–	180.8	–	181.9	–
1′	100.1	4.61, d (7.9)	100.6	4.63, d (7.9)	100.1	4.60, d (7.9)
2′	74.9	3.17, dd (9.2, 7.9)	75.0	3.20, dd (9.1, 7.9)	74.9	3.16, t (8.8)
3′	77.8	3.36, m	77.8	3.40, t (9.1)	77.9	3.36, m
4′	71.6	3.26, m	71.6	3.26, t (9.1)	71.6	3.26, m
5′	78.1	3.27, m	78.1	3.32, o	78.1	3.26, m
6′	62.9	3.85, brd (11.6)	62.9	3.85, m	62.9	3.85, m
		3.63, m		3.62, m		3.63, m
unit B						
1"	55.9	4.25, d (12.3)	56.5	4.16, d (12.7)	55.8	4.25, d (12.5)
		4.20, d (12.3)		3.69, d (12.7)		4.22, d (12.5)
3"	69.3	4.02, dt (9.8, 6.5)	68.7	4.06, m	68.4	3.98, td (9.2, 4.9)
		3.71, dt (9.8, 6.9)		3.75, m		3.62, m
4"	30.8	2.59, m	29.0	2.65, dt (14.3, 7.0)	29.2	2.27, ddd (13.6, 8.5, 5.3)
				2.57, dt (14.3, 5.9)		1.82, ddd (13.6, 9.0, 7.0)
5"	149.0	–	143.5	–	65.2	–
6"	50.2	3.11, m	51.9	2.92, s	45.1	2.12, br d (9.5)
						1.50, d (9.5)
7"	49.6	2.20, d (8.6)	52.5	1.94, br d (8.5)	51.7	2.96, s
		1.43, dd (8.6, 1.5)		1.60, d (9.0)		
8"	62.4	–	62.4	–	150.0	–
9"	145.0	–	144.3	–	140.8	–
10"	14.4	1.29, s	13.0	1.41, s	15.8	1.91, s
1‴	104.6	4.32, d (7.8)	104.0	4.31, d (7.8)	104.7	4.24, d (7.7)
2‴	75.4	3.16, dd (9.0, 7.8)	75.3	3.19, dd (9.0, 7.9)	75.1	3.15, t (8.8)
3‴	77.9	3.36, m	77.9	3.36, o	78.0	3.33, m
4‴	71.9	3.26, m	71.7	3.28, m	71.7	3.26, m
5‴	78.3	3.32, m	78.2	3.28, m	78.3	3.26, m
6‴	62.8	3.88, dd (11.9, 2.2)	62.8	3.86, m	62.8	3.87, m
		3.66, dd (11.9, 6.1)		3.64, m		3.65, m

[a] Assignments are based on COSY, HSQC, and HMBC experiments.

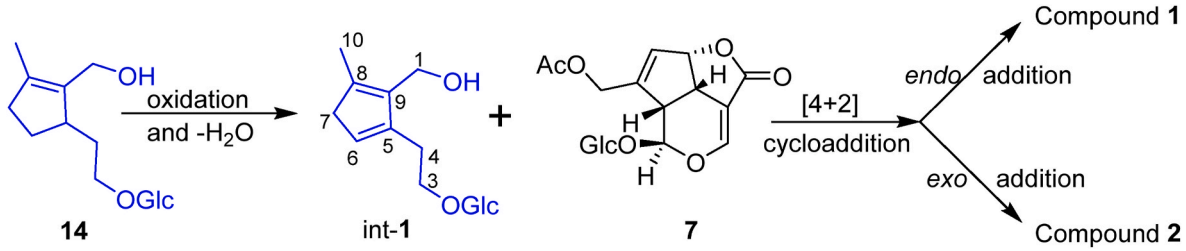

Scheme 1. Biogenetic pathway proposed for compounds **1** and **2**.

between the two datasets, further supporting the correctness of the assignments. The absolute configuration of **3** was deduced to be 1*S*,3*R*,4*R*,5*S*,6*S*,9*S*,5"*S*,7"*S* based on the comparison of the experimental and calculated ECD spectra (Fig. 3c). Accordingly, the structure of **3** was determined as shown and was named phukettoside C.

Compound **4** was isolated as a pale-yellow gum [$[\alpha]_D^{26}$ −8.4, (*c* 1.11, MeOH)]. Its molecular formula was established as $C_{37}H_{48}O_{23}$ from the HRESIMS *m/z* 883.2480 $[M + Na]^+$ (calcd for $C_{37}H_{48}NaO_{23}$ 883.2479) and NMR data, which suggested fourteen degrees of unsaturation. The UV absorption λ_{max} 234 nm supported the presence of an enol-ether system conjugated with a carbonyl group, which is typical for many iridoids (Lee et al., 2004). Similarly, the IR spectrum showed the presence of hydroxy (3361 cm^{-1}), ester (1736 cm^{-1}), and α,β-unsaturated ester (1716 cm^{-1}) groups. Duplication of the signals in both the ^{1}H and ^{13}C-NMR spectra (Table 2 and Figs. S38–S40) preliminarily determined **4** as a dimeric iridoid glycoside. The ^{1}H-NMR spectrum of **4** displayed two anomeric proton signals at δ_H 4.74 (1H, d, J = 7.9 Hz) and 4.73 (1H, d, J = 7.8 Hz), and the resonances in the region δ_H 3.25–4.74, suggested that the two glucosyl units possessed the β-pyranosyl configuration (Table 2). Two sp^2 methine proton signals at δ_H 7.66 (1H, d, J = 0.8 Hz)

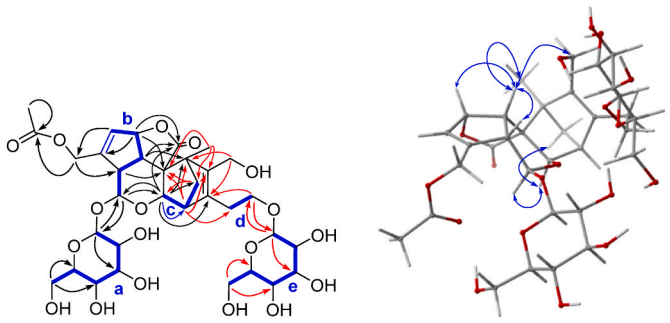

Fig. 2. Key COSY (—), HMBC (⌒), and NOESY (⌒) correlations of **1**.

and 7.69 (1H, d, J = 0.8 Hz), and one methoxy group signal at δ_H 3.74 (3H, s), corresponded to an enol ether system conjugated with a carbomethoxy group (Boros and Stermitz, 1991; Wei et al., 2000; Cai et al., 2021). Two, one-proton singlets at δ_H 6.02 and 6.06 resembled tri-substituted olefins, and overlapping signals attributed to two oxymethine protons at δ_H 4.79 (2H, m) could be observed in the HSQC spectra. The HSQC spectra also displayed two hydroxy methyl groups at δ_H 4.93 (1H, d, J = 14.5 Hz), 4.88 (1H, overlapped with water), and 4.82 (2H, m) and two acetoxy methyl groups at δ_H 2.10 and 2.08. Consistent with these observations, the ^{13}C- and HSQC NMR spectra of **4** revealed 37 signals comprising four carbonyl carbons (δ_C 168.7, 169.4, 172.5, and 172.6), eight olefinic carbons (δ_C 108.0, 108.1, 132.2, 132.7, 145.7, 145.8, 155.4, and 155.8), six oxygenated carbons (δ_C 63.8, 63.8, 75.2, 75.5, 101.5, and 102.0), four sp^3 methine carbons (δ_C 42.3, 42.4, 46.2, and 46.3), together with two anomeric carbons (δ_C 100.7 and 101.1) and oxygenated carbons in the region δ_C 63.0–78.5 belonging to two glucose moieties, and three methyl carbons, including one from a methoxy group (δ_C 20.8, 20.9, and 51.9). These spectroscopic characteristics suggested two structural units in **4**, units **A** and **B**, with both having the daphylloside structure (**8**) (Figs. S64 and S65; Demirezer et al., 2006). The spectral differences were the absence of a methyl ester in unit **B** and the low field shift of the oxymethylene protons (δ_H 4.29 and 4.45) and a carbon (δ_C 64.0, C-6') in the glycosyl moiety of unit **A**, indicating that these structural units were connected through an ester linkage between C-11 of unit **B** and C-6′ of unit **A** (Fig. 1). This linkage was verified by the HMBC correlation (Fig. 6) between the H_2-6′ of unit **A** and C-11 of unit **B**. This structure of compound **4** was further supported by comparing its spectra with those of saprosmoside G (Ling et al., 2002), which belongs to a series of bis-iridoids previously isolated from the Rubiaceae. This structure is comprised of the two deacetylasperulosidic acid units esterified at C-11 of unit **B** and C-6′ of unit **A**, thus confirming a precedence for this type of iridoid dimers. The stereochemical relationships of **4** at C-1, C-5, C-6, and C-9 in each unit were the same as in **8**, as determined through the NOESY spectrum (Fig. 6). Additionally, the coupling constants of *cis* H5/H9*β* and *cis* H-5/H-6 were compared between the experimental ^{1}H-NMR data and the calculated ^{1}H-NMR data (Table S16). This comparison showed a consistent agreement, establishing their stereochemical relationships. The absolute configurations of the two units in **4** were confirmed by the same Cotton effects of their experimental ECD spectra (Fig. 3d and f). Furthermore, the experimental ECD spectrum of **4** fits well with that of the calculated ECD spectrum of 1a*S*,5a*S*,6a*S*,9a*S*,1b*S*,5b*S*,6b*S*,9b*S*-**4** (Fig. 3d), which was named phukettoside D.

Compound **5** was isolated as a pale-yellow gum with $[\alpha]_D^{26}$ +7.0. Its molecular formula was established as $C_{19}H_{26}O_{12}$ based on HRESIMS ([M + Na]$^+$ *m/z* 469.1320 (calcd for $C_{19}H_{26}NaO_{12}$ 469.1317) and NMR spectroscopic data. The UV absorption at λ_{max} 236 nm indicated the presence of an enol-ether system conjugated with a carbonyl group, which is a characteristic feature of many iridoids (Lee et al., 2004). The IR spectrum showed absorption bands due to the presence of hydroxy (3366 cm^{-1}), saturated and *α*,*β*-unsaturated ester carbonyl (1716, 1698 cm^{-1}, respectively), and olefinic (1648 cm^{-1}) functionalities. The ^{1}H-NMR spectrum (Table 2) displayed two olefinic protons at δ_H 7.56 (s) and 5.85 (br s), two oxygenated methine protons at δ_H 4.87 (d, J = 8.8 Hz) and 4.58 (m), a pair of allylic hydroxy methyl protons at δ_H 4.18 (dd, J = 15.5, 3.4 Hz) and 3.98 (dd, J = 15.5, 3.8 Hz), a methoxy group at δ_H 3.63 (s), and a set of characteristic protons attached to oxygen bearing carbons at δ_H 4.56 (d, J = 7.8 Hz, H-1'), 3.01 (td, J = 8.4, 4.9 Hz, H-2'), 3.19 (m, H-3'), 3.09 (td, J = 8.8, 4.0 Hz, H-4'), 3.37 (m, H-5'), 4.14 (dd, J = 11.9, 1.9 Hz, H-6'a), and 4.08 (dd, J = 11.9, 6.5 Hz, H-6'b) ascribable to a *β*-glucosyl moiety. The ^{13}C-NMR and DEPT data (Table 2) revealed 19 carbon resonances, including an acetyl group at δ_C 170.5 (O<u>C</u>OCH$_3$), 20.6 (OCO<u>C</u>H$_3$), a methyl ester group at δ_C 166.9 (<u>C</u>OOCH$_3$), 51.0 (COO<u>C</u>H$_3$), four olefinic carbons at δ_C 153.1 (C-3), 149.2 (C-8), 129.3 (C-7), and 107.3 (C-4), a set of glucosyl resonances at δ_C 99.3 (C-1′), 73.3 (C-2′), 76.3 (C-3′), 70.2 (C-4′). 73.6 (C-5′), and 63.4 (C-6′), three other oxygenated carbons at δ_C 100.4 (C-1), 73.0 (C-6), and 59.7 (C-10), and two sp^3 quaternary carbons at δ_C 41.1 (C-5) and 44.3 (C-9). The ^{1}H and ^{13}C-NMR data of **5** (Table 2) were characteristic of an iridoid glucoside, and closely resembled those of daphylloside (**8**) (Demirezer et al., 2006). The main difference between compound **5** and daphylloside (**8**) was the position of an acetyl group, which changed from C-10 to C-6′. This modification was confirmed by the HMBC correlations from H_2-6' to the acetyl carbonyl group (δ_C 170.5) and C-4' of the glucose unit in compound **5** (Fig. 6). Furthermore, the HMBC correlations between H-1' and C-1, and between H-1 and C-1', indicated that the sugar moiety was located at C-1 of the iridoid aglycone.

Acid hydrolysis of **5** with 2N HCl afforded D-glucose which was identified through co-TLC comparison with an authentic sample and optical rotation [$[\alpha]_D^{26}$ +28.0 (*c* 0.10, H_2O)]. The relative configurations within **5** were established by analysis of the NOESY spectrum (Fig. 6) whereby the correlations between H-5/H-6 and H-5/H-9 indicated that these protons were all *β*-oriented, which corresponded to the structural characteristics of naturally occurring iridoids which have a bicyclic H-5/H-9*β*, *β*-*cis*-fused cyclopentanopyran ring system (Dinda et al., 2011). When compound **5** was stored at 4 °C for several months, deacetylation occurred to produce **6** (co-HPLC with authentic sample). The ECD curves of compounds **5**, **6**, and **8** have similar patterns (Fig. 3f), implying that they share the same absolute configuration. The absolute configurations of **5** were further confirmed by the excellent resemblance of the experimental ECD curve with the calculated ECD curve of the 1*S*,5*S*,6*S*,9*S*-isomer, rather than the *ent*-isomer (Fig. 3e). Accordingly, the absolute configuration of **5** was assigned as 1*S*,5*S*,6*S*,9*S* and **5** was named phukettoside E.

The observed larger coupling constants for *cis* H-5/H-9 and *cis* H-5/H-6 in the iridoid type (Tables 1 and 2) are noteworthy and could be attributed to the dihedral angles between H-5/H-9 and H-5/H-6, which approached 0° within the molecule. The presence of small dihedral angles resulted in enhanced coupling constants for *β*-all *cis* H 5/H-6 and *cis* H-5/H-9 relationships. The optimized conformers were determined using the ωB97XD/cc-PVDZ level of theory. The low-energy conformers of compounds **1**–**5** revealed that the dihedral angles of these conformers fell within the range of 5.1–36.1° (see Fig. S81−S85 and Table S13−S17), confirming that the larger coupling constants are a direct consequence of the near-planar arrangement of these hydrogen atoms in *cis* iridoid glycosides.

The structures of the known compounds were confirmed by comparing their spectral data with the published literature. The isolates include three iridoid glycosides, deacetyl daphylloside (syn. deacetyl asperulosidic acid methyl ester) (**6**) (Demirezer et al., 2006; Inouye et al., 1969; Noiarsa et al., 2008), asperuloside (**7**) (Demirezer et al., 2006; Noiarsa et al., 2008; Otsuka et al., 1991), and daphylloside [syn. asperulosidic acid methyl ester] (**8**) (Demirezer et al., 2006; Lee et al., 2004), two megastigmane glycosides, dihydrovomifoliol-*O*-*β*-D-glucopyranoside (**9**) (Miyase et al., 1988; Andersson and Lundgren, 1988), and vomifoliol-*O*-*β*-D-glucopyranoside (**10**) (Andersson and Lundgren, 1988;

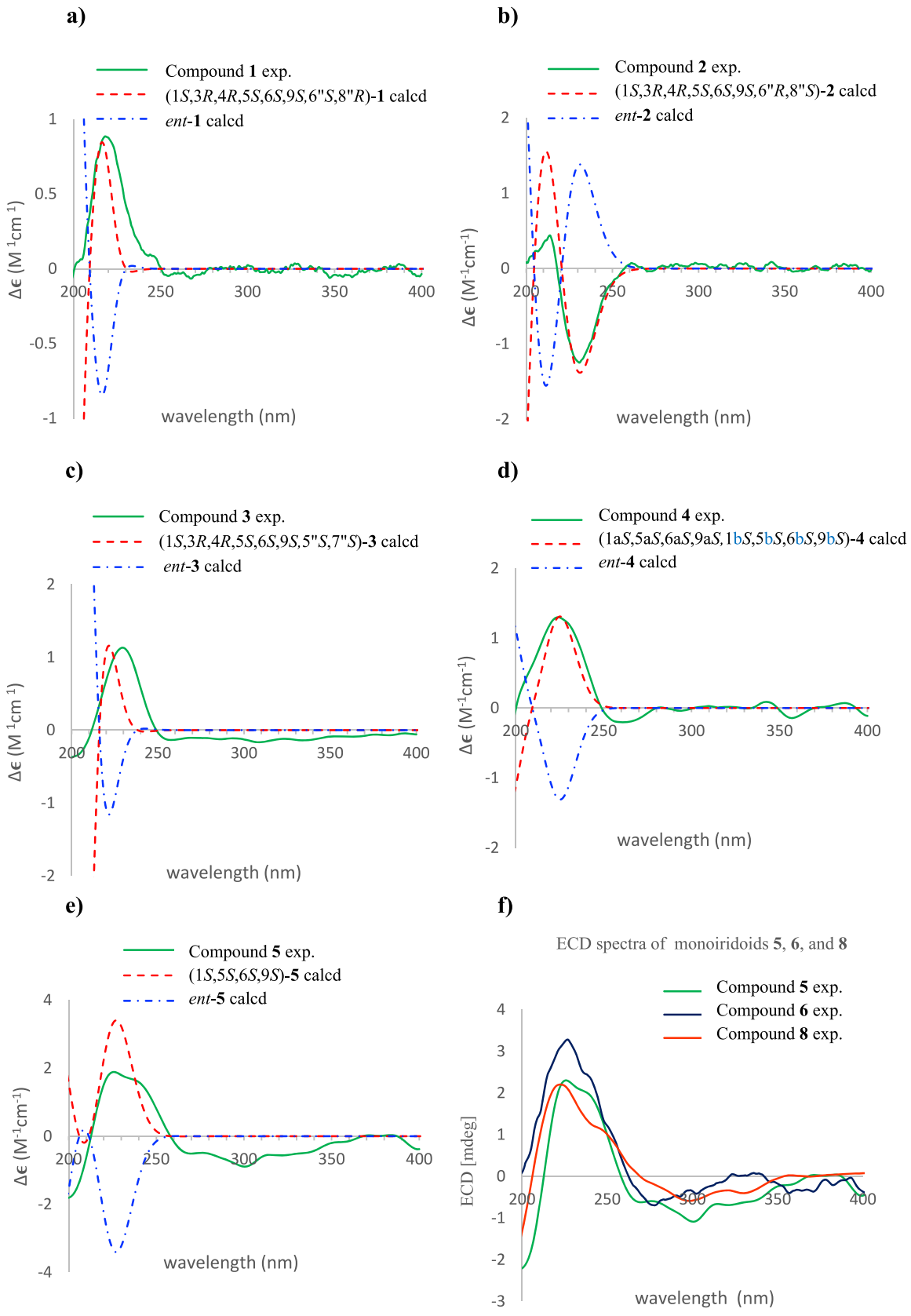

Fig. 3. Experimental and calculated ECD spectra of compounds **1**–**5** (**a**–**e**) and Experimental ECD spectra of **5**, **6**, and **8** (**f**).

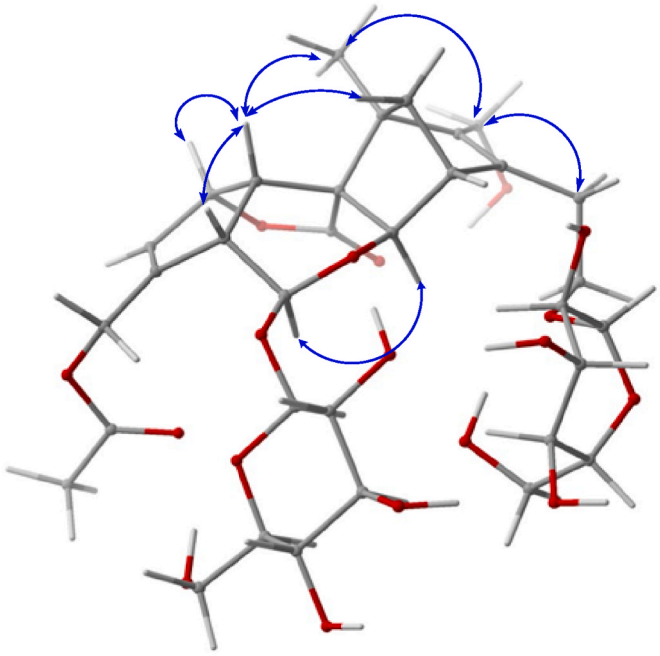

Fig. 4. Key NOESY ( ) correlations of **2**.

Okamura et al., 1981), and three flavonoid glycosides, kaempferol 3-*O*-*β*-D-glucopyranosyl-(1‴→2″)-*α*-L-arabinopyranoside (**11**) (Geller et al., 2014), quercetin 3-*O*-*α*-L-arabinopyranoside (guaijaverin, **12**) (Fraisse et al., 2000) and quercetin 3-*O*-*α*-L-rhamnopyranoside (quercitrin, **13**) (Lee et al., 2004; Park et al., 2011).

Biogenetic pathways for the bis-iridoid glycosides **1**–**3** were proposed through the *endo*- or *exo*-selective [4 + 2]-Diels-Alder cycloaddition reactions between asperuloside (**7**) as a dienophile and intermediate int-**1** or int-**2** derived from kankanoside D (**14**) as a diene partner (Schemes 1 and 2). The allylic hydroxylation and dehydration of kankanoside D (**14**) could produce int-**1** or int-**2**. Diels-Alder reaction of int-**1** with asperuloside (**7**) would generate **1** through an *endo* cycloaddition pathway and **2** through a corresponding *exo* cycloaddition pathway. Likewise, compound **3** would be formed by the *endo*-Diels-Alder cycloaddition of int-**2** with asperuloside (**7**). Notably, this type of bis-derivative structure is described for the first time in a natural iridoid glycoside. The majority of bis-iridoids (as well as bis-iridoid glycosides) reported in the literature are formed through either ester or ether bonds (Boros and Stermitz, 1991; Dinda et al., 2011; Ling et al., 2002; Sang et al., 2003). Nonetheless, the occurrence of Diels-Alder reactions between iridoid glycosides and alkaloids has been documented in the literature. Earlier research conducted by Wang et al. (2013) and Di et al. (2014) had proposed the formation of iridoid glycoside-alkaloid conjugates through [4 + 2]-Diels-Alder cycloaddition reactions, and subsequent synthetic methodology was documented by Zhang et al. (2018).

The isolated compounds were evaluated for their cancer chemopreventive properties and cytotoxic activities. For the cancer chemopreventive properties, the free radical scavenging effects of the isolated compounds were tested on DPPH radicals. Only guaijaverin (**12**) and quercitrin (**13**) showed significant DPPH free radical scavenging effects, with IC_{50} values of 17.7 ± 0.7 and 19.8 ± 0.7 μM, respectively and inhibited superoxide anion radical formation in the xanthine/xanthine oxidase (XXO) assay with IC_{50} values of 41.4 ± 3.1 and 44.4 ± 2.1 μM, respectively (Table S1). The inhibition on the DPPH antioxidant and xanthine-originated superoxide quenching activities of **12** and **13** were previously reported by An et al. (2005) and Park (2011), and the present results are in agreement. Among the isolated compounds no significant inhibition of xanthine oxidase (IXO), inhibition of HL-60 anti-oxidant, inhibition of lipoxygenase (LOX), or inhibition of aromatase (AIA) was observed. For cytotoxic activity assessment, the isolated compounds, except for compounds **2** and **4**, were evaluated with a panel of cancer cell lines including human cholangiocarcinoma (Thai; HuCCA-1), human lung cancer (A549), human cervical carcinoma (HeLa), and human hepatocarcinoma (HepG2), as well as a non-cancerous cell line, human diploid lung fibroblast (MRC-5) (Table S2). No cytotoxic activity was observed for these compounds on either cancer cells or on a normal cell line.

3. Conclusions

In this study, five previously undescribed iridoid glucoside derivatives, named as phukettosides A–E and eight known compounds, were isolated from the leaves of *Morinda umbellata*. The structures of these iridoid glucosides, with their absolute configurations, were determined by NMR spectroscopic data analysis, acid hydrolysis, and quantum chemical calculations. Plausible biogenetic pathways for the bis-iridoid glucosides **1**–**3** were proposed. The isolates were tested for cancer chemoprevention and cytotoxicity, and the results showed that only guaijaverin (**12**) and quercitrin (**13**) displayed moderate DPPH antioxidant and xanthine-xanthine oxidase activities. None of the tested compounds showed cytotoxic activity with cancer cells or a normal human lung fibroblast cell line.

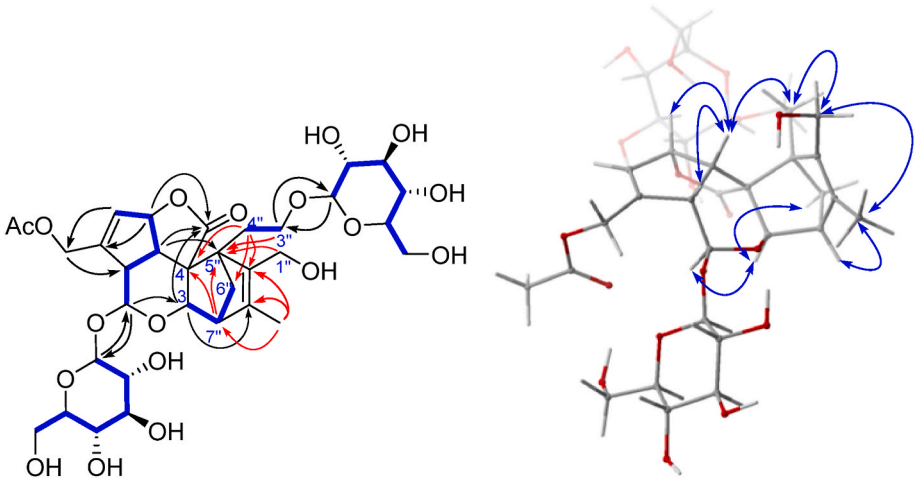

Fig. 5. Key COSY ( ), HMBC ( ), and NOESY ( ) correlations of **3**.

Table 2
^{1}H- (600 MHz) and^{13}C-NMR (150 MHz) NMR spectroscopic data[a] for compounds **4** and **5** (δ in ppm).

Compound	4 (CD_3OD)				5 (DMSO-d_6)	
	unit A		unit B			
Position	δ_C	δ_H, mult. (*J* in Hz)	δ_C	δ_H, mult. (*J* in Hz)	δ_C	δ_H, mult. (*J* in Hz)
1 (CH)	102.0	5.02, d (9.0)	101.5	5.07, d (9.0)	100.4	4.87, d (8.8)
3 (CH)	155.4	7.66, d (0.8)	155.8	7.69, d (0.8)	153.1	7.56, s
4 (C)	108.1	–	108.0	–	107.3	–
5 (CH)	42.3	3.02, br t (7.0)	42.4	3.06, br t (7.0)	41.1	2.83, t (6.2)
6 (CH)	75.2	4.79, m	75.5	4.79, m	73.0	4.58, m
7 (CH)	132.7	6.02, s	132.2	6.06, s	129.3	5.85, br s
8 (C)	145.7	–	145.8	–	149.2	–
9 (CH)	46.2	2.64, br t (7.9)	46.3	2.64, t (7.9)	44.3	2.38, t (8.3)
10 (CH_2)	63.8	4.88, o 4.82, m	63.8	4.93, d (14.5) 4.82, m	59.7	4.18, dd (15.5, 3.4) 3.98, dd (15.5, 3.8)
10-O$\underline{C}$OCH$_3$	172.5	–	172.6	–	–	–
10-OCOC$\underline{H}_3$	20.8	2.08, s	20.9	2.10, s	–	–
11-$\underline{C}$OOCH$_3$	169.4	–	168.7	–	166.9	–
11-COOC$\underline{H}_3$	51.9	3.74, s	–	–	51.0	3.63, s
1′ (CH)	101.1	4.74, d (7.9)	100.7	4.73, d (7.8)	99.3	4.56, d (7.8)
2′ (CH)	75.0	3.26, m	74.9	3.25, m	73.3	3.01, td (8.4, 4.9)
3′ (CH)	78.0	3.38, m	77.7	3.40, m	76.3	3.19, m
4′ (CH)	71.4	3.40, m	71.6	3.28, m	70.2	3.09, td (8.8, 4.0)
5′ (CH)	75.7	3.51, m	78.5	3.28, m	73.6	3.37, m
6′ (CH_2)	64.0	4.45, dd (11.8, 1.8) 4.29, dd (11.8, 4.9)	63.0	3.86, dd (11.8, 1.3) 3.63, dd (12.0, 5.9)	63.4	4.14, dd (11.9, 1.9) 4.08, dd (11.9, 6.5)
6′-O$\underline{C}$OCH$_3$	–	–	–	–	170.5	–
6′-OCOC$\underline{H}_3$	–	–	–	–	20.6	1.97, s

o = overlapping with water.
[a] Assignments are based on COSY, HSQC, and HMBC experiments.

4. Experimental

4.1. General experimental procedures

Optical rotations were recorded on a JASCO DIP 1020 polarimeter. UV spectra were measured with a UV-1700 Pharma Spec Spectrophotometer (Shimadzu, Kyoto, Japan). ECD spectra were performed on a JASCO J-815 Spectropolarimeter (Japan). IR spectra were measured on a PerkinElmer Spectrum One Spectrophotometer using the ATR technique (Massachusetts, USA). HR-MS were performed on a Bruker (Micro TOF-LC) Spectrometer (Bremen, Germany). NMR spectra were recorded on either a Bruker AM 400 or an Advance 600 Spectrometer (Rheinstetten, Germany), using TMS as internal standard. Preparative HPLC was carried out on a Waters 600 system equipped with a Waters Data 600 pump, a Waters 600 Controller, a Waters 2996 photodiode array detector, and Waters Empower 2 software (Massachusetts, USA). A reversed phase Sunfire C18 OBD column (19 × 250 mm, id., 10 μm), was used for separations. Silica gel 60 (Merck, 0.063–0.200 mm) and Sephadex LH-20 (GE Healthcare Bio-Science AB, Uppsala, Sweden) were used for column chromatography (CC). Thin layer chromatography (TLC) was performed on precoated aluminum plates (Merck, silica gel 60 F_{254}).

4.2. Plant material

The leaves of *Morinda umbellata* L. (Rubiaceae) were collected from within Phuket Rajabhat University, Phuket Province, Thailand. in May 2018. The plant was identified by taxonomic staff at the Forest Herbarium, Department of National Parks, Wildlife and Plant Conservation, Bangkok, Thailand. A voucher specimen (CRI 644) was deposited at the Laboratory of Natural Products, Chulabhorn Research Institute, Bangkok, Thailand.

4.3. Extraction and isolation

The air-dried, powdered leaves of *M. umbellata* (3.2 kg) were soaked for 24 h at room temperature with 1:1 CH_2Cl_2–MeOH (3 × 20 L). The solvent extracts were combined and dried under reduced pressure to afford a crude extract (517 g). A sample (500 g) was separated by silica gel CC using a gradient system of hexane–CH_2Cl_2 (20:80 to 0:100) and CH_2Cl_2–MeOH (100:0 to 50:50) to obtain six fractions (A–F). Fraction C (9.09 g), obtained from MeOH–CH_2Cl_2 (10:90), was subjected to Sephadex LH-20 CC eluting with isocratic CH_2Cl_2–MeOH (1:1), to yield five subfractions (C1–C5). Subfraction C5 (2.48 g) was subjected to Sephadex LH-20 CC eluting with MeOH-CH_2Cl_2 (40:60) to give five subfractions (C5.1–C5.5). Subfraction C5.5 (800 mg) was further purified by preparative HPLC (Sunfire C18 eluted with CH_3CN–H_2O from 5:95 to 25:75 over 40 min, flowrate 8 mL/min, detected with λ 224, 236 nm) to afford compounds **5** (25 mg, t_R 27.02 min), **7** (20 mg, t_R 35.6 min), **9** (13.5 mg, t_R 37.8 min), **10** (13 mg, t_R 38.8 min), and **8** (68 mg, t_R 44.03 min). Fraction E (80 g), obtained from MeOH– CH_2Cl_2 (12:88), was fractionated by Sephadex LH-20 CC eluting with MeOH–CH_2Cl_2 (80:20) to obtain four subfractions (E1–E4). Separation of subfraction E2 (28 g) by Sephadex LH-20 CC, eluting with CH_2Cl_2–MeOH (1:1), gave two subfractions (E2.1 and E2.2). Subfraction E2.2 (900 mg) was further purified by preparative HPLC (Sunfire C18, eluted with CH_3CN–H_2O from 5:95 to 25:75 in 50 min, 25:75 to 100:0 in 10 min, flowrate 8 mL/min, detected with λ 224, 236 nm) to afford compounds **3** (9.2 mg, t_R 28.04 min), **2** (6.3 mg, t_R 38.3 min), **6** (13 mg, t_R 39.9 min), **1** (30 mg, t_R 42.14 min), and **4** (11.1 mg, t_R 49.13 min). Subfraction E4 (2.7 g) was separated over Sephadex LH-20, eluting with MeOH–CH_2Cl_2

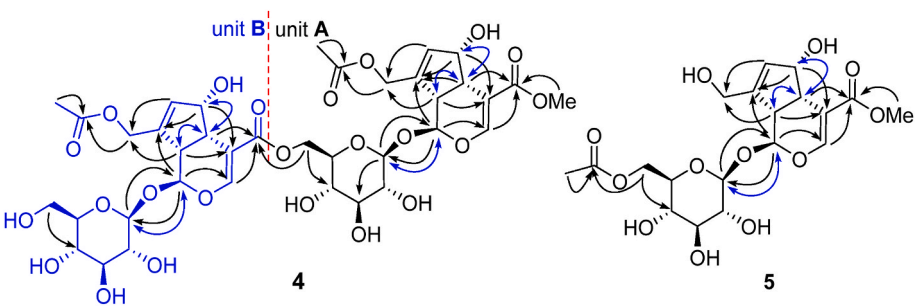

Fig. 6. Key HMBC (⟶) and NOESY (⟷) correlations of compounds **4** and **5**.

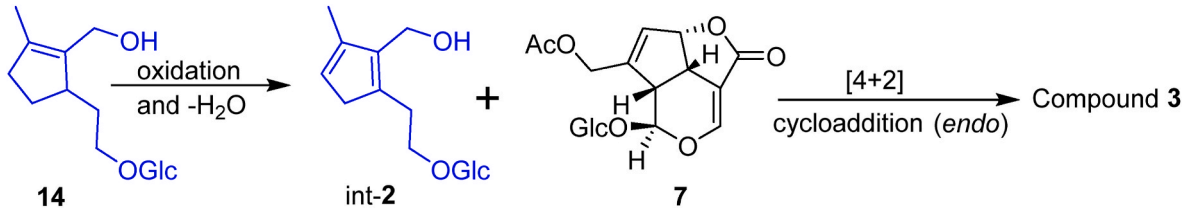

Scheme 2. Biogenetic pathway proposed for compound **3**.

(40:60 → 80:20) to give four subfractions (E4.1–E4.4). Subfraction E4.4 (760 mg) was further purified by preparative HPLC (Sunfire C18, eluted with $CH_3CN–H_2O$, 5:95 to 45:55 in 30 min, flowrate 8 mL/min, detected with λ 224, 236 nm) to afford compounds **11** (50 mg, t_R 23.4 min), **12** (7.2 mg, t_R 25.5 min), and **13** (6.7 mg, t_R 26 min).

4.3.1. Phukettoside A (1)

Pale yellow gum; $[\alpha]_D^{26}$ −75.0 (*c* 0.46, MeOH); UV λ_{max} (MeOH) nm (log ε) 204 (3.8), 276 (2.4); ECD spectrum, see Fig. 3a; IR (ATR) ν_{max} 3359, 3188, 2920, 2851, 1741, 1704, 1659, 1633, 1471, 1424, 1411, 1137, 1378, 721 cm^{-1}; ^1H and ^{13}C-NMR data, see Table 1; HRESIMS *m/z* 753.2585 $[M + Na]^+$ (calcd for $C_{33}H_{46}NaO_{18}$ 753.2576; Δ = −1.1).

4.3.2. Phukettoside B (2)

Pale yellow gum; $[\alpha]_D^{26}$ −71.3 (*c* 0.39, MeOH); UV λ_{max} (MeOH) nm (log ε) 203 (3.5); ECD spectrum, see Fig. 3b; IR (ATR) ν_{max} 3360, 3193, 2921, 2852, 1741, 1722, 1659, 1634, 1470, 1378, 1168, 721 cm^{-1}; ^1H and ^{13}C-NMR data, see Table 1; HRESIMS *m/z* 765.2367 $[M + Cl]^-$ (calcd for $C_{33}H_{46}O_{18}Cl$ 765.2378; Δ = 1.4).

4.3.3. Phukettoside C (3)

Pale yellow gum; $[\alpha]_D^{26}$ −56.8 (*c* 0.24, MeOH); UV λ_{max} (MeOH) nm (log ε) 203 (3.6), 225 (sh); ECD spectrum, see Fig. 3c; IR (ATR) ν_{max} 3359, 3193, 2922, 2852, 1740, 1717, 1659, 1633, 1469, 1378, 1171, 721 cm^{-1}; ^1H and ^{13}C-NMR data, see Table 1; HRESIMS *m/z* 753.2573 $[M + Na]^+$ (calcd for $C_{33}H_{46}NaO_{18}$ 753.2576; Δ = 0.4).

4.3.4. Phukettoside D (4)

Pale yellow gum; $[\alpha]_D^{26}$ −8.4 (*c* 1.11, MeOH); UV λ_{max} (MeOH) nm (log ε) 204 (3.6), 234 (3.6); ECD spectrum, see Fig. 3d; IR (ATR) ν_{max} 3361, 3196, 2921, 2852, 1736, 1716, 1658, 1634, 1470, 1378, 1245, 1079, 1052, 721 cm^{-1}; ^1H and ^{13}C-NMR data, see Table 2; HRESIMS *m/z* 883.2480 $[M + Na]^+$ (calcd for $C_{37}H_{48}NaO_{23}$ 883.2479; Δ = −0.10).

4.3.5. Phukettoside E (5)

Pale yellow gum; $[\alpha]_D^{26}$ +7.0 (*c* 1.69, MeOH); UV λ_{max} (MeOH) nm (log ε) 236 (3.9); ECD spectrum, see Fig. 3e; IR (ATR) ν_{max} 3366, 2924, 2854, 1716, 1698, 1648, 1608, 1443, 1367, 1200, 1167, 1087, 1056, 954, 817, 787 cm^{-1}; ^1H and ^{13}C-NMR data, see Table 2; HRESIMS *m/z* 469.1320 $[M + Na]^+$ (calcd for $C_{19}H_{26}NaO_{12}$ 469.1317; Δ = 0.75).

4.4. Acid hydrolysis of compounds 1 and 5

Compound **1** (1.8 mg) was dissolved in 2N HCl (0.5 mL) and heated at 60 °C for 2 h. Water was added, and the reaction mixture extracted with CH_2Cl_2 (3 × 2 mL). The aqueous phase was evaporated under vacuum to yield an off-white solid, which was identified as D-glucose by TLC comparison with standard sugar samples and by its optical rotation $[\alpha]_D^{25}$ +25.0 (*c* 0.08, H_2O). The same operating procedure was used for compound **5**, affording D-glucose with $[\alpha]_D^{26}$ +28.0 (*c* 0.1, H_2O).

4.5. Chemoprevention assays

Radical scavenging potential was performed by reaction with 1,1-diphenyl-2-picrylhydrazyl (DPPH) free radicals, as described by Van Amsterdam et al. (1992). Ascorbic acid was used as the reference compound and showed a half-maximal scavenging concentration (IC_{50}) of 32.2 ± 2.0 μM (Table S1). Inhibition of 12-*O*-tetradecanoylphorbol-13-acetate (TPA)-induced superoxide anion radical generation in differentiated HL-60 cells (HL-60 antioxidant) was detected by photometric determination of cytochrome C reduction, as previously described by Gerhäuser et al. (2003). Superoxide dismutase (SOD; 60U) served as a positive control. Cell viability was examined in parallel to avoid false positive results. Only the tested compounds with >50% cell viability were considered for calculation of the scavenging potential (Table S1). Inhibition of xanthine oxidase activity (IXO) was determined by quantifying the amount of uric acid produced from xanthine. The method described by Rangkadilok et al. (2007) was followed using allopurinol as a positive control, which inhibited xanthine oxidase with an IC_{50} value of 4.6 ± 0.4 μM (Table S1). Inhibition of superoxide radical formation by xanthine/xanthine oxidase (XXO) was detected indirectly by measuring the rate of reduced XTT production as described by Gerhäuser et al. (2003). Gallic acid was the positive control, exhibiting an IC_{50} value of 2.9 ± 0.2 μM. The IC_{50} value of XXO was determined only when the XXO activity of the tested compounds was greater than the IXO activity (Table S1). Inhibition of lipoxygenase activity (LOX) was performed by measuring leukotriene metabolites as described by Gleason et al. (1995). Nordihydroguaiaretic acid, as the positive control, inhibited lipoxygenase activity with an IC_{50} value of 4.5 ± 0.5 μM (Table S1). Inhibition of aromatase (AIA) was performed using the method designed by Stresser et al. (2000). The reference compound, letrozole, inhibited CYP19 with an IC_{50} value of 1.4 ± 0.3 nM (Table S1).

4.6. Cytotoxicity assay

Cytotoxic activity was evaluated according to established procedures (Kheawchaum et al., 2022). Briefly, cytotoxic activity for adhesive cell lines, including human cholangiocarcinoma (Thai; HuCCA-1), human lung cancer (A549), human cervical carcinoma (HeLa), human hepatocarcinoma (HepG2), and human breast cancer (MDA-MB-231) cell lines, was evaluated using the MTT assay. For the non-adhesive T-lymphoblast (MOLT-3) cell line, the cytotoxicity was assessed using the XTT assay. The cytotoxicity results were reported as % cytotoxic activity at the given concentration (see Table S2). The finding was performed by preparing the initial concentration at 50 μg/mL. Then, the initial concentration was systematically diluted until the solution became clear. The percentage of cytotoxic activity was determined at these specific concentrations (50, 25, 10, or 5 μg/mL), and the concentration unit was converted to micromolar, as shown in Table S2 (SI). In this study, the IC_{50} value was not performed because the % cytotoxic activities of the tested compounds were lower than 50%. Etoposide was used as the positive control for the MOLT-3 cell line with an IC_{50} value of 0.018 ± 0.004 μM. Doxorubicin was used as the positive control for the HuCCA-1, A549, HeLa, HepG2, MDA-MB-231, and MRC-5 cell lines and displayed IC_{50} values of 0.79 ± 0.08, 0.19 ± 0.007, 0.16 ± 0.07, 0.33 ± 0.05, 1.18 ± 0.07, and 1.31 ± 0.13 μM, respectively.

4.7. Calculation methods

The conformational search was performed using Conformer–Rotamer Ensemble Sampling Tool (CREST) with the iMTD-GC conformational search algorithm and the GBSA solvent model of methanol (Grimme 2019; Pracht et al., 2020). All DFT calculations were performed using the Gaussian 16 Rev. C.01 program (Dennington et al., 2016; Frisch et al., 2016). The low-energy conformers within an energy window of 3 kcal/mol were further optimized at ωB97XD/cc-PVDZ level of theory with the IEFPCM of methanol solvent model. All optimized conformers were confirmed as the true minimum of electronic potential energy by calculation of the vibrational frequencies at the same level, and no imaginary frequencies were detected. According to the Boltzmann distribution based on Gibbs free energies, each conformer with a population over 2% was subjected to ECD calculations. The simulated ECD spectra of **1**−**5** were executed using TD-DFT at the M06-2x/def2-SVP level of theory with IEFPCM of methanol solvent model (Weigend, 2006; Weigend and Ahlrichs, 2005; Zhao and Truhlar, 2008). For each conformer, 30 excited states were calculated and the simulated ECD curves were generated using SpecDis with Boltzmann averaging of all conformers and overlapping Gaussian function with an exponential half-width ($\sigma = 0.35$) (Bruhn et al., 2013, 2017). Theoretical ECD spectra of the related enantiomers were generated from the direct inversion of simulated ECD spectra as shown in Fig. 3a–e and SI pages 47−60.

The coupling constants ($J_{H,H}$) for the ^{1}H-NMR were calculated for the low-energy conformers using the ωB97XD/cc-PVDZ level of theory. These calculations were performed at the B3LYP/6-31G(d,p)u+1s level, considering only the Fermi contact term, and scaled using the slope parameter 0.9115 (Rablen and Bally, 2011) (see SI pages 61−63).

Declaration of competing interest

The authors declare that they have no known competing financial interests or personal relationships that could have appeared to influence the work reported in this paper.

Data availability

Data will be made available on request.

Acknowledgments

This research work was supported in part by the Thailand Science Research and Innovation (TSRI), Chulabhorn Research Institute (Grant No. 36824/4274394 and 36827/4274406), and the Center of Excellence on Environmental Health and Toxicology (EHT), OPS, Ministry of Higher Education, Science, Research and Innovation. The authors thank the CRI staff members, Pakamas Intachote, Suchada Sengsai, Somkid Sitthimonchai, and Busakorn Saimanee for the antiproliferative activity determinations. We are pleased to thank Kittiporn Trisuppakant, and Nitirat Chimnoi for spectral data collection. The authors thank Prof. Emeritus Geoffrey A. Cordell, Natural Products Inc., Evanston, IL, USA for assisting in the revision of this manuscript.

Appendix A. Supplementary data

Supplementary data to this article can be found online at https://doi.org/10.1016/j.phytochem.2023.113890.

References

An, R.B., Kim, H.C., Tian, Y.H., Kim, Y.C., 2005. Free radical scavenging and hepatoprotective constituents from the leaves of *Juglans sinensis*. Arch Pharm. Res. (Seoul) 28, 529–533. https://doi.org/10.1007/BF02977753.

Akihisa, T., Matsumoto, K., Tokuda, H., Yasukawa, K., Seino, K.-I., Nakamoto, K., Kuninaga, H., Suzuki, T., Kimura, Y., 2007. Anti-inflammatory and potential cancer chemopreventive constituents of the fruits of *Morinda citrifolia* (Noni). J. Nat. Prod. 70, 754–757. https://doi.org/10.1021/np068065o.

Andersson, R., Lundgren, N.L., 1988. Monoaryl and cyclohexenone glycosides from needles of Pinus sylvestris. Phytochemistry 27, 559–562. https://doi.org/10.1016/003-9422(88)83141-8.

Ban, N.K., Giang, V.H., Linh, T.M., Linh, L.Q., Ngoc, N.T., Thao, D.T., Nam, N.H., Cuong, N.X., Kiem, P.V., Minh, C.V., 2013. Two new 11-noriridoids from the aerial parts of *Morinda umbellata*. Phytochem. Lett. 6, 267–269. https://doi.org/10.1016/j.phytol.2013.03.011.

Boros, C.A., Stermitz, F.R., 1991. Iridoids. An updated review, part II. J. Nat. Prod. 54, 1173–1246. https://doi.org/10.1021/np50077a001.

Bruhn, T., Schaumlöffel, A., Hemberger, Y., Bringmann, G., 2013. SpecDis: quantifying the comparison of calculated and experimental electronic circular dichroism spectra. Chirality 25, 243–249. https://doi.org/10.1002/chir.22138.

Bruhn, T., Schaumlöffel, A., Hemberger, Y., Pescitelli, G., 2017. *SpecDis*, Ver. 1.71. Berlin, Germany.

Burnett, A.R., Thomson, R.H., 1968. Anthraquinones in *Morinda umbellata* L. Phytochemistry 7, 1421–1422. https://doi.org/10.1016/S0031-9422(00)85651-4.

Cai, M., Liu, M., Chen, H., Wang, Y., Yang, D., 2021. Iridoids with anti-inflammatory effect from the aerial parts of *Morinda officinalis* How. Fitoterapia 153, 104991. https://doi.org/10.1016/j.fitote.2021.104991.

Chang, P., Chen, C.-F., 1995. Isolation and characterization of antitumor anthraquinones from *Morinda umbellata*. Chin. Pharmaceut. J. 47, 347–353.

Chiou, C.T., Hsu, R.Y., Lin, L.C., 2014. Isolation and cytotoxic effect of anthraquinones from *Morinda umbellata*. Planta Med. 80, 1113–1117. https://doi.org/10.1055/s-0034-1382956.

Dalsgaard, P.W., Potterat, O., Dieterle, F., Paululat, T., Kühn, T., Hamburger, M., 2006. Noniosides E–H, new trisaccharide fatty acid esters from the fruit of *Morinda citrifolia* (Noni). Planta Med. 72, 1322–1327. https://doi.org/10.1055/s-2006-951706.

Demirezer, L.Ö., Gürbüz, F., Güvenalp, Z., Ströch, K., Zeeck, A., 2006. Iridoids, flavonoids and monoterpene glycosides from *Galium verum* subsp. verum. Turk. J. Chem. 30, 525–534. https://journals.tubitak.gov.tr/chem/vol30/iss4/13.

Deng, S., Palu, A.K., West, B.J., Su, C.X., Zhou, B.-N., Jensen, J.C., 2007. Lipoxygenase inhibitory constituents of the fruits of noni (*Morinda citrifolia*) collected in Tahiti. J. Nat. Prod. 70, 859–862. https://doi.org/10.1021/np0605539.

Dennington, R., Keith, T.A., Millam, J.M., 2016. GaussView, Version 6. Semichem Inc., Shawnee Mission, KS. https://gaussian.com/gaussview6/.

Di, Y.-T., Wee, C.-S., Li, C.-S., Kong, N.-C., Wang, J.-S., Fang, X., Zhu, H.-J., Wu, Y.-D., Hao, X.-J., 2014. Longphyllinesides A and B: natural Diels-Alder adducts from *Daphniphyllum longeracemosum*? Tetrahedron 70, 4017–4021. https://doi.org/10.1016/j.tet.2014.04.073.

Dinda, B., Debnath, S., Rajarshi Banik, R., 2011. Naturally occurring iridoids and secoiridoids. An updated review, part 4. Chem. Pharm. Bull. 59, 803–833. https://doi.org/10.1248/cpb.59.803.

Fraisse, D., Heitz, A., Carnet, A., Carnet, A.-P., Lamaison, J.-L., 2000. Quercetin 3-arabinopyranoside, a major flavonoid compound from *Alchemilla xanthochlora*. Fitoterapia 71, 463–464. https://doi.org/10.1016/S0367-326X(00)00145-3.

Frisch, M.J., Trucks, G.W., Schlegel, H.B., Scuseria, G.E., Robb, M.A., Cheeseman, J.R., Scalmani, G., Barone, V., Petersson, G.A., Nakatsuji, H., Li, X., Caricato, M., Marenich, A.V., Bloino, J., Janesko, B.G., Gomperts, R., Mennucci, B., Hratchian, H. P., Ortiz, J.V., Izmaylov, A.F., Sonnenberg, J.L., Williams-Young, D., Ding, F., Lipparini, F., Egidi, F., Goings, J., Peng, B., Petrone, A., Henderson, T., Ranasinghe, D., Zakrzewski, V.G., Gao, J., Rega, N., Zheng, G., Liang, W., Hada, M., Ehara, M., Toyota, K., Fukuda, R., Hasegawa, J., Ishida, M., Nakajima, T., Honda, Y., Kitao, O., Nakai, H., Vreven, T., Throssell, K., Montgomery Jr., J.A., Peralta, J.E., Ogliaro, F., Bearpark, M.J., Heyd, J.J., Brothers, E.N., Kudin, K.N., Staroverov, V.N., Keith, T.A., Kobayashi, R., Normand, J., Raghavachari, K., Rendell, A.P., Burant, J. C., Iyengar, S.S., Tomasi, J., Cossi, M., Millam, J.M., Klene, M., Adamo, C., Cammi, R., Ochterski, J.W., Martin, R.L., Morokuma, K., Farkas, O., Foresman, J.B., Fox, D.J., 2016. Gaussian 16, Revision C.01. Gaussian, Inc., Wallingford CT. https://gaussian.com/gaussian16/.

Geller, F., Murillo, R., Steinhauser, L., Heinsmann, B., Albert, K., Merfort, I., Laufer, S., 2014. Four new flavonol glycosides from the leaves of *Brugmansia suaveolens*. Molecules 19, 6727–6736. https://doi.org/10.3390/molecules19056727.

Gerhäuser, C., Klimo, K., Heiss, E., Neumann, I., Gamal-Eldeen, A., Knauft, J., Liu, G.Y., Sitthimonchai, S., Frank, N., 2003. Mechanism-based *in vitro* screening of potential cancer chemopreventive agents. Mutat. Res. 523–524, 163–172. https://doi.org/10.1016/S0027-5107(02)00332-9.

Gleason, M.M., Rojas, C.J., Learn, K.S., Perrone, M.H., Bilder, G.E., 1995. Characterization and inhibition of 15-lipoxygenase in human monocytes: comparison with soybean 15-lipoxygenase. Am. J. Physiol. 268, C1301–C1307. https://doi.org/10.1152/ajpcell.1995.268.5.c1301.

Grimme, S., 2019. Exploration of chemical compound, conformer, and reaction space with meta-dynamics simulations based on tight-binding quantum chemical calculations. J. Chem. Theor. Comput. 15, 2847–2862. https://doi.org/10.1021/acs.jctc.9b00143.

Hashim, Y., Toume, K., Mizukami, S., Ge, Y.-W., Taniguchi, M., Teklemichael, A.A., Huy, N.T., Bodi, J.M., Hirayama, K., Komatsu, K., 2021. Phenylpropanoid conjugated iridoids with anti-malarial activity from the leaves of *Morinda morindoides*. J. Nat. Med. 75, 915–925. https://doi.org/10.1007/s11418-021-01541-x.

Ismail, T.S., Sulthana, A.P., 2008. Standardization of *Morinda umbellata* Linn. - an effective crude drug for diarrhea. E-J. Chem. 5, 652–658. https://doi.org/10.1155/2008/376568.

Kanchanapoom, T., Kasai, R., Yamasaki, K., 2002. Iridoid and phenolic glycosides from Morinda coreia. Phytochemistry 59, 551–556. https://doi.org/10.1016/S0031-9422(01)00426-5.

Kesonbuaa, W., Chantaranothai, P., 2013. The genus *Morinda* (Rubiaceae) in Thailand. Sci. Asia 39, 331–339. https://doi.org/10.2306/scienceasia1513-1874.2013.39.331.

Kheawchaum, S., Mahidol, C., Thongnest, S., Boonsombat, J., Batsomboon, P., Sitthimonchai, S., Ruchirawat, S., Prawat, H., 2022. *Ent*-abietane diterpenoid lactone glycosides and a phenolic glycoside from *Phlogacanthus pulcherrimus* T. Anderson with cytotoxic and cancer chemopreventive activities. Phytochemistry 201, 113261. https://doi.org/10.1016/j.phytochem.2022.113261.

Lee, J.H., Ku, C.H., Baek, N.-l., Kim, S.-H., Park, H.W., Kim, D.K., 2004. Phytochemical constituents from *Diodia teres*. Arch Pharm. Res. (Seoul) 27, 40–43. https://doi.org/10.1007/BF02980043.

Li, C., Dong, C., Li, F., Fu, J., Xie, J., Lai, S., Wang, H., Chen, R., Kang, J., 2021. The racemic trimeric quinone and polycyclic quinones isolated from the aerial parts of *Morinda umbellata* L. Phytochemistry 183, 112622. https://doi.org/10.1016/j.phytochem.2020.112622.

Li, C., Su, X., Li, F., Fu, J., Wang, H., Li, B., Chen, R., Kang, J., 2019. Cytotoxic quinones from the aerial parts of *Morinda umbellata* L. Phytochemistry 167, 112096. https://doi.org/10.1016/j.phytochem.2019.112096.

Li, C., Wang, H., Dong, C., Xie, J., Lai, S., Liu, J., Chen, R., Kang, J., 2022. New quinones, a sesquiterpene and phenol compounds with cytotoxic activity from the aerial parts of *Morinda umbellata* L. Fitoterapia 156, 105089. https://doi.org/10.1016/j.fitote.2021.105089.

Ling, S.-K., Komorita, A., Tanaka, T., Fujioka, T., Mihashi, K., Kouno, I., 2002. Iridoids and anthraquinones from the Malaysian medicinal plant, *Saprosma scortechinii* (Rubiaceae). Chem. Pharm. Bull. 50, 1035–1040. https://doi.org/10.1248/cpb.50.1035.

Miyase, Y., Ueno, A., Takizawa, N., Kobayashi, H., Oguchi, H., 1988. Studies on the glycosides of *Epimedium grandiflorum* Morr. Var. *thunbergianum* (Miq.) Nakai. III. Chem. Pharm. Bull. 36, 2475–2484. https://doi.org/10.1248/cpb.36.2475.

Noiarsa, P., Ruchirawat, S., Otsuka, H., Kanchanapoom, T., 2008. Chemical constituents from *Oldenlandia corymbosa* L. of Thai origin. J. Nat. Med. 62, 249–250. https://doi.org/10.1007/s11418-007-0212-1.

Oladeji, O.S., Oluyori, A.P., Dada, A.O., 2022. Genus *Morinda*: an insight to its ethnopharmacology, phytochemistry, pharmacology and industrial applications. Arab. J. Chem. 15, 104024 https://doi.org/10.1016/j.arabjc.2022.104024.

Otsuka, H., Yoshimura, K., Yamasaki, K., Cantoria, M.C., 1991. Isolation of 10-*O*-acyl iridoid glucosides from a Philippine medicinal plant, *Oldenlandia corymbosa* L. (Rubiaceae). Chem. Pharm. Bull. 39, 2049–2052. https://doi.org/10.1248/cpb.39.2049.

Okamura, N., Yagi, A., Nishioka, I., 1981. Studies on the constituents of Zizyphi fructus. V. structures of glycosides of benzyl alcohol, vomifoliol and naringenin. Chem. Pharm. Bull. 29, 3507–3514. https://doi.org/10.1248/cpb.29.3507.

Park, S., Yang, S., Ahn, D., Yang, J.H., Kim, D.K., 2011. Antioxidative phenolic compounds from the whole plant of *Juncus diastrophanthus*. J. Korean Soc. Appl. Biol. Chem. 54, 685–692. https://doi.org/10.1007/BF03253146.

Pracht, P., Bohle, F., Grimme, S., 2020. Automated exploration of the low-energy chemical space with fast quantum chemical methods. Phys. Chem. Chem. Phys. 22, 7169–7192. https://doi.org/10.1039/C9CP06869D.

Rablen, P.R., Bally, T., 2011. Quantum-chemical simulation of ^{1}H NMR spectra. 2. comparison of DFT-based procedures for computing proton–proton coupling constants in organic molecules. J. Org. Chem. 76, 4818–4830. https://doi.org/10.1021/jo200513q.

Rangkadilok, N., Sitthimonchai, S., Worasuttayangkurn, L., Mahidol, C., Ruchirawat, M., Satayavivad, J., 2007. Evaluation of free radical scavenging and antityrosinase activities of standardized longan fruit extract. Food Chem. Toxicol. 45, 328–336. https://doi.org/10.1016/j.fct.2006.08.022.

Razafimandimbison, S.G., Bremer, B., 2011. Nomenclatural changes and taxonomic notes in the tribe Morindeae (Rubiaceae). Adansonia 33, 283–309.

Sang, S., Cheng, X., Zhu, N., Stark, R.E., Badmaev, V., Ghai, G., Rosen, R.T., Ho, C.-T., 2001. Flavonol glycosides and novel iridoid glycoside from the leaves of *Morinda citrifolia*. J. Agric. Food Chem. 49, 4478–4481. https://doi.org/10.1021/jf010492e.

Sang, S., Liu, G., He, K., Zhu, N., Dong, Z., Zheng, Q., Rosen, R.T., Ho, C.-T., 2003. New unusual iridoids from the leaves of noni (*Morinda citrifolia* L.) show inhibitory effect on ultraviolet B-induced transcriptional activator protein-1 (AP-1) activity. Bioorg. Med. Chem. 11, 2499–2502. https://doi.org/10.1016/S0968-0896(03)00180-9.

Stresser, D.M., Turner, S.D., McNamara, J., Stocker, P., Miller, V.P., Crespi, C.L., Patten, C.J., 2000. A high-throughput screen to identify inhibitors of aromatase (CYP19). Anal. Biochem. 284, 427–430. https://doi.org/10.1006/abio.2000.4729.

Su, B.-N., Pawlus, A.D., Jung, H.-A., Keller, W.J., McLaughlin, J.L., Kinghor, A.D., 2005. Chemical constituents of the fruits of *Morinda citrifolia* (Noni) and their antioxidant activity. J. Nat. Prod. 68, 592–595. https://doi.org/10.1021/np0495985.

Van Amsterdam, F.T.M., Roveri, A., Maiorino, M., Ratti, E., Ursini, F., 1992. Lacidipine: a dihydropyridine calcium antagonist with antioxidant activity. Free Radic. Biol. Med. 12, 183–187. https://doi.org/10.1016/0891-5849(92)90025-c.

Wang, F., Mao, M.-F., Wei, G.-Z., Gao, Y., Ren, F.-C., Liu, J.-K., 2013. Hybridaphniphyllines A and B, daphniphyllum alkaloid and iridoid hybrids suggestive of Diels–Alder cycloaddition in *Daphniphyllum longeracemosum*. Phytochemistry 95, 428–435. https://doi.org/10.1016/j.phytochem.2013.07.005.

Wei, X., Xie, H., Ge, X., Zhang, F., 2000. Iridoids from *Dunnia sinensis*. Phytochemistry 53, 837–840. https://doi.org/10.1016/s0031-9422(99)00581-6.

Weigend, F., 2006. Accurate Coulomb-fitting basis sets for H to Rn. Phys. Chem. Chem. Phys. 8, 1057–1065. https://doi.org/10.1039/B515623H.

Weigend, F., Ahlrichs, R., 2005. Balanced basis sets of split valence, triple zeta valence and quadruple zeta valence quality for H to Rn: design and assessment of accuracy. Phys. Chem. Chem. Phys. 7, 3297–3305. https://doi.org/10.1039/B508541A.

Xie, H., Morikawa, T., Matsuda, H., Nakamura, S., Muraoka, O., Yoshikawa, M., 2006. Monoterpene constituents from *Cistanche tubulosa* – chemical structures of kankanosides A–E and kankanol. Chem. Pharm. Bull. 54, 669–675. https://doi.org/10.1248/cpb.54.669.

Zandi, L., Makungu, M., Munissi, J.J.E., Duffy, S., Puttreddy, R., von der Heiden, D., Rissanen, K., Avery, V.M., Nyandoro, S.S., Erdélyi, M., 2020. Secoiridoids and iridoids from *Morinda asteroscepa*. J. Nat. Prod. 83, 2641–2646. https://doi.org/10.1021/acs.jnatprod.0c00447.

Zhang, W., Ding, M., Li, J., Guo, Z., Lu, M., Chen, Y., Liu, L., Shen, Y.-H., Li, A., 2018. Total synthesis of hybridaphniphylline B. J. Am. Chem. Soc. 140, 4227–4231. https://doi.org/10.1021/jacs.8b01681.

Zhao, Y., Truhlar, D.G., 2008. The M06 suite of density functionals for main group thermochemistry, thermochemical kinetics, noncovalent interactions, excited states, and transition elements: two new functionals and systematic testing of four M06-class functionals and 12 other functionals. Theor. Chem. Acc. 120, 215–241. https://doi.org/10.1007/s00214-007-0310-x.